

# Nonreciprocal Spin Waves Driven by Left-Hand Microwaves

Zhizhi Zhang, Zhenyu Wang, Huanhuan Yang, Z.-X. Li, Yunshan Cao, and Peng Yan\*

School of Electronic Science and Engineering and State Key Laboratory of Electronic Thin Films and Integrated Devices, University of Electronic Science and Technology of China, Chengdu 610054, China

It is a conventional wisdom that a left-hand microwave cannot efficiently excite the spin wave (SW) in ferromagnets, due to the constraint of angular momentum conservation. In this work, we show that the left-hand microwave can drive nonreciprocal SWs in the presence of a strong ellipticity-mismatch between the microwave and precessing magnetization. A critical frequency is predicted, at which the left-hand microwave cannot excite SWs. Away from it the SW amplitude sensitively depends on the ellipticity of left-hand microwaves, in sharp contrast to the case driven by right-hand ones. By tuning the microwave frequency, we observe a switchable SW non-reciprocity in a ferromagnetic single layer. A mode-dependent mutual demagnetizing factor is proposed to explain this finding. Our work advances the understanding of the photon-magnon conversion, and paves the way to designing diode-like functionalities in nano-scaled magnonics.

*Introduction.*—Magnonics is an emerging field aiming for the future low-loss wave-based computation [1–7]. Among the splendid magnonic functionalities, chirality and non-reciprocity serve as the basic building blocks [8–12] for the integrated magnonic circuits since the spin precession is innately chiral [13–15]. The non-reciprocity can root in the magneto-dipolar interaction via, for example, the well known Damon-Eshbach (DE) geometry [16–19], bilayer magnet and inhomogeneous thin film [20–27], and magnetic heterostructure in the presence of magneto-elastic or magneto-optic coupling [28–31]. However, with the isotropic exchange interaction dominating in the microscale region [32–34], the dipolar effects, followed by the induced non-reciprocity, are vanishingly small [35]. The non-reciprocity can also emerge in the chiral edge states of elaborately devised topological magnetic materials or spin-texture arrays, which are robust to defects and disorders [36–41]. But it requires specific lattice designs and complicated couplings between atoms or elements, and the confined magnon (the quantum of spin wave) channels at the edges reduce the usage of the magnetic systems. Another origin for the non-reciprocity comes from the Dzyaloshinskii-Moriya interaction (DMI) [42]. Yet, the effect is negligibly weak in ferromagnetic insulators, like yttrium iron garnet (YIG,  $\text{Y}_3\text{Fe}_5\text{O}_{12}$ ) [43]. Additional heavy metal structures can introduce a sizable DMI [44–46], but inevitably bring remarkably increased damping and Joule heating [47].

To realize an efficient excitation of the non-reciprocal short-wavelength dipolar-exchange or even pure exchange spin waves (SWs) in ferromagnetic insulators for miniaturizing magnonic devices, several promising methods have been suggested [48–54]. Conventionally, the coherent SW excitation harnesses the microwave antennas with the exciting field linearly polarized and uniform across the film thickness. Since the in-plane component of microwave fields dominantly contributes to the excitations, it is solely accounted in the analysis [55–58]. By contrast, the dynamic fields generated by micro-magnetic structures are not only highly localized at interfaces favoring the short-wavelength SWs excitation [59–61], but also polarized with complex chiralities. Recently, Yu *et al.* have reported an analysis for the chiral pumping (excitation) of exchange magnons in YIG into (from) the proximate

magnetic wires via directional dipolar interactions [62, 63]. A selection rule is adopted that circular magnons and photons with the same (opposite) chiralities are allowed (forbidden) to interact [30]. One critical issue noteworthy rises how the microwave fields with contrary chirality excite the propagating SWs.

In this work, we theoretically investigate the propagating SWs in ferromagnetic films excited by microwave fields with generic chiralities. We find that the left-hand microwave can excite SWs because of the ellipticity mismatch between microwave and dynamic magnetization, which extrapolates the aforementioned selection rule for the magnon-photon conversion. Since the contributions of the in-plane and out-of-plane components of left- (right-) hand microwave fields are destructive (constructive) superposed, we introduce an analog to the common and differential signals in the differential amplifier. Surprisingly, we find a critical frequency where no SWs can be excited by left-hand microwaves. We propose a proof-of-concept strategy for generating non-reciprocal SWs via applying the left-hand local microwave unevenly across the film thickness. A directional mutual demagnetizing factor is suggested to understand the emerging switchable SW chirality that depends on the microwave frequency. This proposal makes full use of the magnetic structures without breaking the symmetry of the dispersion relations and increasing the damping, which is superior to other methods. Our work lays a foundation of employing the chiral excitation for magnonic diodes in nano scales.

*Model and analysis.*—We consider a ferromagnetic layer YIG with nanometer thickness  $d$  extended in the  $x-z$  plane and magnetized along  $z$  direction [see Fig. 1(a)]. The magnetic parameters of YIG are  $M_s = 1.48 \times 10^5$  A/m,  $A_{ex} = 3.1 \times 10^{-12}$  J/m, and  $\alpha = 5 \times 10^{-4}$  [64]. The microwave field for the SWs excitation is centered at  $x = 0$  and located in the region with the width  $w$ . The micromagnetic simulations are performed using MuMax3 [65] to verify the derived theories (see Supplemental Material Sec. I [66]).

The magnetization dynamics is governed by Landau-

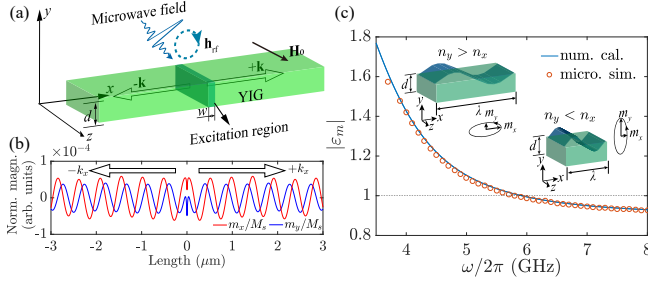


FIG. 1: (a) Schematic of the chiral excitation of SWs with a coordinate system and geometric parameters. The chiral microwave field  $\mathbf{h}_{rf}$  is locally applied in the patched green region. The SWs are propagating along  $x$  direction indicated by the hollow arrows. (b) Spatial distribution of normalized dynamic magnetization  $[m_{x(y)}/M_s]$  at 4 GHz at an arbitrary time slot. The blue (red) curves represent the  $x$  ( $y$ ) component. The microwave is left-circularly polarized and uniform across the film thickness. (c) Frequency dependence of the dynamic magnetization ellipticity ( $\epsilon_m$ ). Solid curves are calculated based on Eq. (8). Circles are the micromagnetic simulations. Insets: Schematic illustrations of the spin-precessing cones for  $n_y > n_x$  and  $n_y < n_x$ , respectively.

Lifshitz-Gilbert (LLG) equation

$$\frac{\partial \mathbf{M}}{\partial t} = -\gamma \mu_0 \mathbf{M} \times \mathbf{H}_{\text{eff}} + \frac{\alpha}{M_s} \mathbf{M} \times \frac{\partial \mathbf{M}}{\partial t}, \quad (1)$$

where  $\gamma$  is the gyromagnetic ratio,  $\mu_0$  is the vacuum permeability,  $\alpha \ll 1$  is the dimensionless Gilbert damping constant,  $M_s$  is the saturated magnetization,  $\mathbf{M} = \mathbf{m} + M_s \mathbf{z}$  is the magnetization with  $\mathbf{m} = m_x \mathbf{x} + m_y \mathbf{y}$  the dynamic component, and  $\mathbf{H}_{\text{eff}} = \mathbf{H}_0 + \mathbf{h}_{rf} + \mathbf{h}_{ex} + \mathbf{h}_d$  with  $\mathbf{H}_0 = H_0 \mathbf{z}$  ( $\mathbf{h}_{rf} = h_x \mathbf{x} + h_y \mathbf{y}$ ) the bias (microwave) magnetic field,  $\mathbf{h}_{ex} = (2A/\mu_0 M_s^2) \nabla^2 \mathbf{m}$  the exchange field where  $A$  is the exchange constant, and  $\mathbf{h}_d$  being the dipolar field satisfying the magneto-static Maxwell's equation  $\nabla \cdot (\mathbf{h}_d + \mathbf{m}) = 0$  and  $\nabla \times \mathbf{h}_d = 0$ . The free boundary conditions at the top and bottom surfaces require  $\partial m_{x(y)}/\partial y|_{y=0,-d} = 0$  [67]. Thus, only the first unpinned mode with uniform profile of dynamic magnetization across the thickness exists in the low frequency band due to the ultra thin thickness [68]. We assume a plane-wave form  $\mathbf{m} = \mathbf{m}_0 e^{j(\omega t - k_x x)}$  with  $\mathbf{m}_0 = m_{x0} \mathbf{x} + m_{y0} \mathbf{y}$  and  $m_{x(y)} = m_{x0(y0)} e^{j(\omega t - k_x x)}$ . Substituting these terms into Eq. (1) and adopting the linear approximation, we obtain

$$j\omega m_x + (j\alpha\omega + \omega_y) m_y = \omega_M h_y, \quad (2a)$$

$$-(j\alpha\omega + \omega_x) m_x + j\omega m_y = -\omega_M h_x, \quad (2b)$$

where  $\omega_x = n_x \omega_M + \omega_H + \omega_{ex}$  and  $\omega_y = n_y \omega_M + \omega_H + \omega_{ex}$ , with  $\omega_M = \gamma \mu_0 M_s$ ,  $\omega_H = \gamma \mu_0 H_0$ , and  $\omega_{ex} = (2\gamma A/M_s) k_x^2$ . The demagnetizing factors  $n_x$  and  $n_y$  of  $\mathbf{h}_d = -n_x m_x \mathbf{x} - n_y m_y \mathbf{y}$  are given by (see Supplemental Material Sec. II A [66])

$$n_x = 1 - n_y = 1 - \frac{1 - e^{-|k_x|d}}{|k_x|d}. \quad (3)$$

The dispersion relation can be obtained by neglecting the damping term ( $\alpha = 0$ ) and setting  $\mathbf{h}_{rf} = 0$  in Eqs. (2), which

leads to:

$$\omega = \sqrt{\omega_x \omega_y}. \quad (4)$$

The SW dispersion relation with  $d = 40$  nm and  $H_0 = 52$  mT (same hereinafter) obtained from simulation shows only one band exists in the low frequency range from 3 to 8 GHz, whose profile across the thickness is uniform (see Supplemental Material Sec. III [66]). Factors  $n_x$  and  $n_y$  in Eq. (3) are uniquely describing the SW mode with uniform transverse profile [66], quite different with those of other SW modes with much higher frequencies [69]. Solving Eqs. (2), we obtain:

$$m_x = \chi_y(k_x, \omega) h_x + j\kappa(k_x, \omega) h_y, \quad (5a)$$

$$m_y = -j\kappa(k_x, \omega) h_x + \chi_x(k_x, \omega) h_y, \quad (5b)$$

where

$$\chi_x(k_x, \omega) = -\frac{(\omega_x + j\alpha\omega)\omega_M}{\omega^2 - (\omega_x + j\alpha\omega)(\omega_y + j\alpha\omega)}, \quad (6a)$$

$$\chi_y(k_x, \omega) = -\frac{(\omega_y + j\alpha\omega)\omega_M}{\omega^2 - (\omega_x + j\alpha\omega)(\omega_y + j\alpha\omega)}, \quad (6b)$$

$$\kappa(k_x, \omega) = -\frac{\omega\omega_M}{\omega^2 - (\omega_x + j\alpha\omega)(\omega_y + j\alpha\omega)}. \quad (6c)$$

The coefficients  $\chi_x(k_x, \omega)$ ,  $\chi_y(k_x, \omega)$  and  $\kappa(k_x, \omega)$  possess the same denominator, whose absolute value takes the minimum when the dispersion relation Eq. (4) is satisfied. It means that even though the microwave field comprises multiple wave vector components within  $2\pi/w$  [54, 64], only the SWs with  $k_x$  and  $\omega$  satisfying Eq. (4) can be efficiently excited. Substituting Eq. (4) into Eqs. (6) and neglecting the higher-order terms, the magnetic parameters reduce to

$$\chi_x = -\frac{j\omega_x \omega_M}{\alpha(\omega_x + \omega_y) \sqrt{\omega_x \omega_y}}, \quad (7a)$$

$$\chi_y = -\frac{j\omega_y \omega_M}{\alpha(\omega_x + \omega_y) \sqrt{\omega_x \omega_y}}, \quad (7b)$$

$$\kappa = -\frac{j\omega_M}{\alpha(\omega_x + \omega_y)}. \quad (7c)$$

Substituting Eqs. (7) into Eqs. (5), we obtained the ratio between the  $x$  and  $y$  components of the dynamic magnetization as below

$$\epsilon_m = \frac{m_x}{m_y} = j \sqrt{\frac{\omega_y}{\omega_x}}. \quad (8)$$

Equation (8) delivers following features of spin precessions: (i) the imaginary unit  $j$  in  $\epsilon_m$  implies spin precessions in ferromagnetic films are always right-hand polarized, as shown in Fig. 1(b) where  $m_y$  drops behind  $m_x$  for 1/4 wavelength regardless of their propagating directions. (ii) The  $\epsilon_m$  is irrelevant to the amplitudes or phases of  $h_x$  and  $h_y$ . In the exchange limit of  $k_x \rightarrow \infty$ ,  $\epsilon_m \rightarrow j$  indicates the SWs are perfectly right-circularly polarized [70]. Meanwhile, in the dipolar-exchange region where the dipolar effect is comparable to exchange interaction,  $\epsilon_m$  varies with factors  $n_x$  and  $n_y$ , which rely on  $(\omega, k_x)$ , as shown in Fig. 1(c).

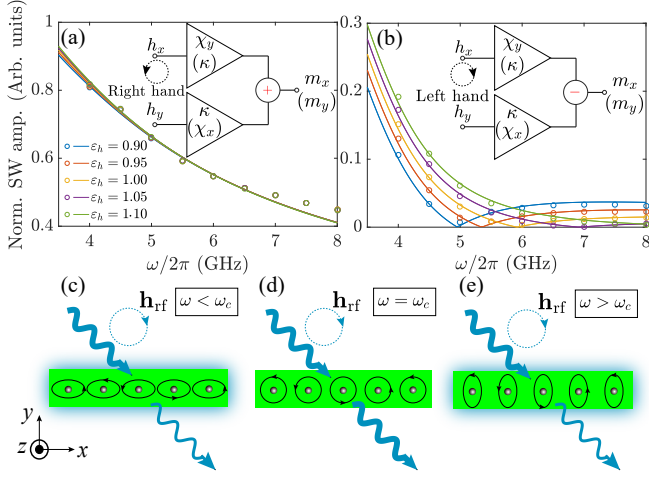


FIG. 2: SW amplitudes ( $|\mathbf{m}|$ ) normalized by the maximal value excited by (a) the right- and (b) left-hand chiral microwave fields with the same power density but different ellipticities ranging from 0.9 to 1.1. Solid curves are calculated based on Eqs. (5). Insets in (a) and (b) depict the schematics of constructive and destructive superposition of the contributions of  $h_x$  and  $h_y$ , in analog to the common and different signals in differential amplifiers, respectively. Symbols are from micromagnetic simulations. Illustrations of the left-hand chiral photon-magnon conversion (c) below, (d) at and (e) above  $\omega_c$ . The blue wavy arrays are the exciting fields with thickness indicating the intensity. The dots and circles represent the spins and their precession cones, respectively.

Below, we discuss the contributions of  $h_x$  and  $h_y$  to the SW amplitude  $|\mathbf{m}| = \sqrt{m_x^2 + m_y^2}$ . Microwave fields  $h_x = j\epsilon_h h_y$  and  $h_x = -j\epsilon_h h_y$  represents respectively the right- and left-handed polarization with  $\epsilon_h$  being their ellipticity. We fix the value of  $h_x^2 + h_y^2$  to ensure the same power density and alter  $\epsilon_h$  to tune the ellipticity. The amplitude spectra of the SWs excited by the right- and left-hand polarized microwaves with  $\epsilon_h$  ranging from 0.9 to 1.1 are plotted in Figs. 2(a) and 2(b), respectively.

The chiral excitation of SWs possesses the following features. Firstly, the complex parameters  $\chi_x, \chi_y$  and  $\kappa$  expressed by Eqs. (7) take the same phase factor. Therefore, Eqs. (5) manifest that the contribution of  $h_y$  to  $\mathbf{m}$  is delayed by the phase of  $\pi/2$  compared to that of  $h_x$ . Consequently, they are superposed destructively (constructively) in the case of left-(right-) hand excitation. Simulation results confirm this point that the left-hand excited SW intensities are weaker than its right-hand counterpart. Secondly, the left-hand excited SW intensities are far more sensitive to the variation of  $\epsilon_h$  than the right-hand excited ones. It is observed that the curves describing different  $\epsilon_h$  in Fig. 2(a) are almost merged, while those in Fig. 2(b) are well separated. We introduce an analog to the differential amplifier in electronic systems [71], where the different (common) mode signal is sensitive (irresponsive) to the tiny variation ( $\epsilon_h$ ) of the dual inputs ( $h_x$  and  $h_y$ ), as illustrated by the insets in Figs. 2(a) and 2(b). Lastly, the ratios between the contributions of  $h_x$  and  $h_y$  to  $m_x$  and  $m_y$  are both  $\chi_x/\kappa = \kappa/\chi_y = \sqrt{\omega_x/\omega_y} = 1/|\epsilon_m|$ . It suggests a critical fre-

quency ( $\omega_c$ ) exists when  $|\epsilon_m| = 1/\epsilon_h$ , at (below and above) which the left-hand microwave is unable (able) to excite any SWs, as illustrated by Figs. 2(c), 2(d) and 2(e). We emphasize that the coincidentally equal ratios are vital for supporting the critical frequencies, since it enables the simultaneous complete offsets of the contributions of microwave field components to the two dynamic magnetization components, and hence the zero SW amplitudes. Meanwhile, the equality of the ratios ensures that  $\epsilon_m$  is intrinsically independent on the polarization and the intensity of the microwave fields, as discussed above. It is also the prerequisite for treating SWs as scalar variables in previous researches [72–74]. This finding broadens the selection rule for photon-magnon conversion, which is instructive to the chiral magneto-optic and -acoustic effects [30, 75]. However,  $\omega_c$  cannot exist for arbitrary  $\epsilon_h$  because  $|\epsilon_m|$  can only take values from 0.91 to 2.14 in the present model. Consequently,  $\omega_c$  can only emerge with  $\epsilon_h$  in the range from 0.47 to 1.09. Analytical and numerical results indeed confirm this point that the curve for  $\epsilon_h = 1.1$  (the green one) in Fig. 2(b) cannot intersect with  $x$  axis.

The above discussions implicate that using the left-hand excitation is essential to generate the non-reciprocal SWs. One critical technique is to differentiate the ellipticity ( $\epsilon_h^+$  and  $\epsilon_h^-$ ) of microwave fields for exciting the forward and backward propagating SWs (symbols “+” and “−” are used to label the forward and backward parameters, respectively, same hereinafter). In preceding works, since the micro-magnets outside YIG films do not constitute the spin-wave guides, the effective exciting polarizations are simply circular [50, 51, 62, 63, 70]. Here, we propose a novel method by applying microwave field unevenly across the film thickness, where the source magnets are parts of the spin-wave guides. Below, a semi-analytic analysis is presented to explain the non-reciprocity. For simplification, we adopt an elementary model that the microwave field is uniformly applied only on the top of the film with thickness  $d_1$ , as shown in Fig. 3(a). We make the approximation that dynamic magnetizations ( $\mathbf{m}_1 = m_{x,1}\mathbf{x} + m_{y,1}\mathbf{y}$  and  $\mathbf{m}_2 = m_{x,2}\mathbf{x} + m_{y,2}\mathbf{y}$ ) along  $d_1$  and  $d_2 = d - d_1$  are transversely uniform. The part in dashed red box taking bilayer structure is regarded as the SW source. In this case, the dipolar fields are composed of two components: the self demagnetizing field  $\mathbf{h}_{d,p} = -n_{x,p}m_{x,p}\mathbf{x} - n_{y,p}m_{y,p}\mathbf{y}$  where  $n_{x(y),p}$  is given by Eq. (3) with  $n_{x(y)} \rightarrow n_{x(y),p}$  and  $d \rightarrow d_p$ , and the mutual demagnetizing field  $\mathbf{h}_{d,pq} = h_{d,x,pq}\mathbf{x} + h_{d,y,pq}\mathbf{y}$  [ $(p, q) = (1, 2)$  or  $(2, 1)$ ]. Here  $h_{d,x(y),pq}$  satisfy the following identity (see Supplemental Material, Sec. II B [66])

$$\begin{bmatrix} h_{d,x,pq} \\ h_{d,y,pq} \end{bmatrix} = -n_{pq} \begin{bmatrix} 1 & j\text{sgn}(k_x)(q-p) \\ j\text{sgn}(k_x)(q-p) & -1 \end{bmatrix} \begin{bmatrix} m_{x,p} \\ m_{y,p} \end{bmatrix}, \quad (9)$$

with

$$n_{pq} = \frac{(1 - e^{-|k_x|d_p})(1 - e^{-|k_x|d_q})}{2|k_x|d_q}. \quad (10)$$

The  $\mathbf{h}_{d,pq}$  ( $\mathbf{h}_{d,p}$ ) is directionally dependent (independent) according to Eqs. (9) [Eq. (3)]. Hence, it is  $\mathbf{h}_{d,pq}$  that contributes

to the non-reciprocity rather than  $\mathbf{h}_{d,p}$ . In addition,  $\mathbf{h}_{d,21}^+$  ( $\mathbf{h}_{d,21}^-$ ) and  $\mathbf{h}_{d,12}^+$  ( $\mathbf{h}_{d,12}^-$ ) are contrarily circular polarized with different intensities, as sketched in the inset of Fig. 3(a) [as proved by

$$\mathbf{h}_{d,\text{mut}} = \frac{\mathbf{h}_{d,12}d_2 + \mathbf{h}_{d,21}d_1}{d} = -n_{\text{mut}} \left\{ \left[ (m_{x,1} + m_{x,2}) + j\text{sgn}(k_x)(m_{y,1} - m_{y,2}) \right] \mathbf{x} + \left[ j\text{sgn}(k_x)(m_{x,1} - m_{x,2}) - (m_{y,1} + m_{y,2}) \right] \mathbf{y} \right\}. \quad (11)$$

with

$$n_{\text{mut}} = \frac{(1 - e^{-|k_x|d_1})(1 - e^{-|k_x|d_2})}{2|k_x|d}. \quad (12)$$

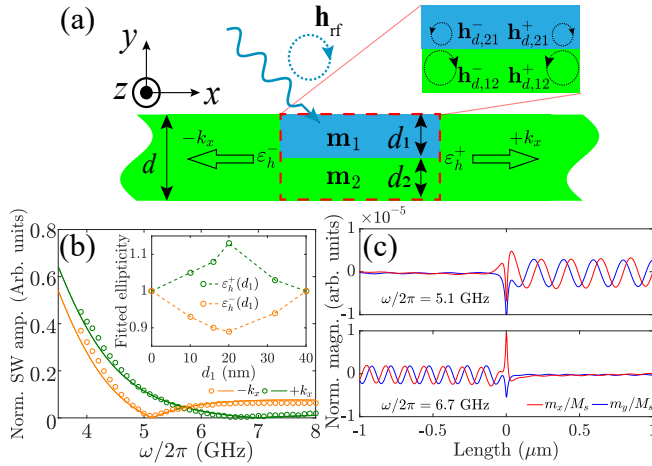


FIG. 3: (a) The schematic for the non-reciprocal SW excitation using left-hand chiral microwave field applied on the top half of the film in the patched blue area. Inset shows the precession cones of the mutual dipolar fields induced by the forward and backward propagating SWs in each layer, with the amplitude indicated by the radius. (b) Spectra of the forward (green curves) and backward (orange curves) SWs amplitudes with excitation depths  $d_1 = 20$  nm. The intensities are normalized with the maximal value. Symbols are numerical simulations and the curves are the fitting results. The inset of (b) shows the fitted  $\varepsilon_h^+(d_1)$  and  $\varepsilon_h^-(d_1)$  dependence on  $d_1$ . (c) The simulated  $m_x/M_s$  and  $m_y/M_s$  distribution at two critical frequencies,  $\omega/2\pi = 5.1$  and 6.7 GHz, respectively.

Following conclusions can thus be drawn. Firstly, the non-reciprocity disappear if  $d_1 = 0$  or  $d_2 = 0$ , which causes  $n_{\text{mut}} = 0$  and  $\mathbf{h}_{d,\text{mut}} = 0$ . It was confirmed that the SWs propagating along opposite directions share the same amplitude with the uniform excitation across the thickness, as shown in Fig. 1(b). Secondly, since  $\mathbf{h}_{d,\text{mut}}$  is determined by  $\mathbf{m}_1$  and  $\mathbf{m}_2$ , its role is to tune the two gains in the differential amplifier [insets of Figs. 2(a) and 2(b)], equivalent to varying  $\varepsilon_h$  of the input microwave  $\mathbf{h}_{rf}$ . As the variation of  $\varepsilon_h$  is directional with  $\mathbf{h}_{d,\text{mut}}$ , the intensity spectra are well separated for the forward and backward SWs, as plotted in Fig. 3 (b). Even though  $\mathbf{h}_{d,\text{mut}}$  is a frequency-dependent parameter, simulation results

Eqs. (27) in Supplemental Material]. The net effective mutual field  $\mathbf{h}_{d,\text{mut}}$  on the entire film is therefore given by

can still be well fitted using Eqs. (5) and  $h_x = -j\varepsilon_h^{+(-)}(d_1)h_y$  with  $\omega_c$  satisfying  $\varepsilon_h^{+(-)}(d_1)|\varepsilon_m| = 1$ , where  $\varepsilon_h^{+(-)}(d_1)$  is the effective ellipticity to be determined. The fitted  $\varepsilon_h^{+(-)}(d_1)$  is plotted in the inset of Fig. 3(b). Representatively, we obtain  $\varepsilon_h^+(10 \text{ nm}) = 1.05$  and  $\varepsilon_h^-(10 \text{ nm}) = 0.93$ , corresponding to  $\omega_c/2\pi = 5.1$  and 6.7 GHz, where the dynamic magnetization is presented in upper and lower panels of Fig. 3(c), respectively, demonstrating the switchable non-reciprocity. Thirdly, the difference between  $\varepsilon_h^+$  and  $\varepsilon_h^-$  and the separation of the forward and backward SW intensity spectra approaches the maximum at  $d_1 = d_2 = d/2$ , meeting the maximal value condition of  $n_{\text{mut}}$  in Eq. (12). For a 20 nm case,  $\varepsilon_h^+ = 1.13$  indicates that the perfect backward SW propagation with zero forward SW cannot be achieved. Lastly, for completeness, we perform the simulations using right-hand and linear excitation, where the forward and backward SW spectra are not well separated as presented in Supplemental Material Sec. IV [66], indicating a negligible contribution of DE mechanism to the non-reciprocity in the left-hand excitation configuration. Moreover, the forward SWs are always stronger than the backward ones in the whole frequency band, implying that DE mechanism induced nonreciprocity cannot be switched by tuning frequencies since it is merely dependent on the surface normal and static magnetization directions [18, 19].

Finally, we note that the microwave field unevenly across the film thickness can be generated by the spin nano-oscillators with various structures, like the nano-disk [76] or the nano-wire [77]. To obtain the desired field distribution, their geometries need to be devised. The switched non-reciprocity at two critical frequencies can also facilitate the exploration of magnonic frequency division multiplexing [78]. Furthermore, the exchange interaction between the micro-magnetic structures and the SW guides can be a promising candidate since it is rather localized and much stronger than the dipolar effects, where the ferro- or antiferro-magnetic exchange coupling combined with the biased magnetization can tune the excitation chirality [67].

*Conclusion.*—In summary, we investigated the propagating dipolar-exchange SWs excited by chiral microwaves in ferro-magnetic thin films. We showed that the left-hand microwave can excite non-reciprocal SWs in the condition of ellipticity mismatch. When the left-hand microwave is unevenly applied across the film thickness, we observed a SW chirality switching by tuning the microwave frequency. Our findings shine a



new light on the photon-magnon conversion and pave the way toward engineering the nano-scaled chiral microwave field for the realization of the diode-like functionalities in magnonics.

*Acknowledgements.*—We thank Y. Henry for helpful discussions. This work was supported by the National Natural Science Foundation of China (NSFC) (Grants No. 12074057, No. 11604041, and No. 11704060). Z.Z. acknowledges the financial support of the China Postdoctoral Science Foundation under Grant No. 2020M673180. Z.W. acknowledges the financial support of the China Postdoctoral Science Foundation under Grant No. 2019M653063. Z.-X.L. acknowledges financial support from the China Postdoctoral Science Foundation (Grant No. 2019M663461) and the NSFC (Grant No. 11904048).

---

\* Corresponding author: [yan@uestc.edu.cn](mailto:yan@uestc.edu.cn)

- [1] A. Barman, G. Gubbiotti, S. Ladak, A. O. Adeyeye, M. Krawczyk, J. Gräfe, C. Adelman, S. Cotoana, A. Naemi, V. I. Vasyuchka, B. Hillebrands, S. A. Nikitov, H. Yu, D. Grundler, A. Sadovnikov, A. A. Grachev, S. E. Sheshukova, J.-Y. Duquesne, M. Marangolo, C. Gyorgy et al. The 2021 Magnonics Roadmap, *J. Phys.: Condens. Matter* **33**, 413001 (2021).
- [2] A. Mahmoud, F. Ciubotaru, F. Vanderveken, A. V. Chumak, S. Hamdioui, C. Adelman, and S. Cotoana, Introduction to spin wave computing, *J. Appl. Phys.* **128**, 161101 (2020).
- [3] V. E. Demidov, S. Urazhdin, G. de Loubens, O. Klein, V. Cros, A. Anane, and S. O. Demokritov, Magnetization oscillations and waves driven by pure spin currents, *Phys. Rep.* **673**, 1 (2017).
- [4] D. Grundler, Nanomagnonics around the corner, *Nat. Nanotechnol.* **11**, 407 (2016).
- [5] A. V. Chumak, V. I. Vasyuchka, A. A. Serga and B. Hillebrands, Magnon spintronics, *Nat. Phys.* **11**, 453 (2015).
- [6] B. Lenk, H. Ulrichs, F. Garbs, M. Münzenberg, Magnon spintronics, *Phys. Rep.* **507**, 107 (2010).
- [7] A. A. Serga, A. V. Chumak and B. Hillebrands, YIG magnonics, *J. Phys. D: Appl. Phys.* **43**, 264002 (2010).
- [8] J. Chen, H. Wang, T. Hula, C. Liu, S. Liu, T. Liu, H. Jia, Q. Song, C. Guo, Y. Zhang, J. Zhang, X. Han, D. Yu, M. Wu, H. Schultheiss, and H. Yu, Reconfigurable Spin-Wave Interferometer at the Nanoscale, *Nano Lett.* **21**, 14 (2021).
- [9] K. Szulc, P. Graczyk, M. Mruczkiewicz, G. Gubbiotti, and M. Krawczyk, Spin-Wave Diode and Circulator Based on Unidirectional Coupling, *Phys. Rev. Applied* **14**, 034063 (2020).
- [10] M. Grassi, M. Geilen, D. Louis, M. Mohseni, T. Brächer, M. Hehn, D. Stoeffler, M. Bailleul, P. Pirro, and Y. Henry, Slow-Wave-Based Nanomagnonic Diode, *Phys. Rev. Applied* **14**, 024047 (2020).
- [11] J. Lan, W. Yu, R. Wu, and J. Xiao, Spin-Wave Diode, *Phys. Rev. X* **5**, 041049 (2015).
- [12] M. Jamali, J. H. Kwon, S.-M. Seo, K.-J. Lee and H. Yang, Spin wave nonreciprocity for logic device applications, *Sci. Rep.* **3**, 3160 (2013).
- [13] P. Pirro, V. I. Vasyuchka, A. A. Serga, and B. Hillebrands, Advances in coherent magnonics, *Nat. Rev. Mater.* **66**, 38 (2021).
- [14] V. V. Kruglyak, Chiral magnonic resonators: Rediscovering the basic magnetic chirality in magnonics, *Appl. Phys. Lett.* **119**, 200502 (2021).
- [15] V. V. Kruglyak, S. O. Demokritov and D. Grundler, Magnonics, *J. Phys. D: Appl. Phys.* **43**, 264001 (2010).
- [16] R. W. Damon and J. R. Eshbach, Magnetostatic modes of a ferromagnet slab, *J. Phys. Chem. Solids* **19**, 308 (1961).
- [17] R. E. Camley, Nonreciprocal surface waves, *Surf. Sci. Rep.* **7**, 103 (1987).
- [18] J. H. Kwon, J. Yoon, P. Deorani, J. M. Lee, J. Sinha, K. J. Lee, M. Hayashi, and H. Yang, Giant nonreciprocal emission of spin waves in Ta/Py bilayers, *Sci. Adv.* **2**, e1501892 (2016).
- [19] T. An, V. I. Vasyuchka, K. Uchida, A. V. Chumak, K. Yamaguchi, K. Harii, J. Ohe, M. B. Jungfleisch, Y. Kajiwara, H. Adachi, B. Hillebrands, S. Maekawa, and E. Saitoh, Unidirectional spin-wave heat conveyer, *Nat. Mater.* **12**, 549 (2013).
- [20] M. Ishibashi, Y. Shiota, T. Li, S. Funada, T. Moriyama, and T. Ono, Switchable giant nonreciprocal frequency shift of propagating spin waves in synthetic antiferromagnets, *Sci. Adv.* **6**, eaaz6931 (2020).
- [21] R. A. Gallardo, T. Schneider, A. K. Chaurasiya, A. Oelschlägel, S. S. P. K. Arekapudi, A. Roldán-Molina, R. Hübner, K. Lenz, A. Barman, J. Fassbender, J. Lindner, O. Hellwig, and P. Landeros, Reconfigurable Spin-Wave Nonreciprocity Induced by Dipolar Interaction in a Coupled Ferromagnetic Bilayer, *Phys. Rev. Applied* **12**, 034012 (2019).
- [22] K. An, V.S. Bhat, M. Mruczkiewicz, C. Dubs, and D. Grundler, Optimization of Spin-Wave Propagation with Enhanced Group Velocities by Exchange-Coupled Ferrimagnet-Ferromagnet Bilayers, *Phys. Rev. Applied* **11**, 034065 (2019).
- [23] O. Gladii, M. Haidar, Y. Henry, M. Kostylev, and M. Bailleul, Frequency nonreciprocity of surface spin wave in permalloy thin films, *Phys. Rev. B* **93**, 054430 (2016).
- [24] R. A. Gallardo, P. Alvarado-Seguel, T. Schneider, C. Gonzalez-Fuentes, A. Roldan-Molina, K. Lenz, J. Lindner, and P. Landeros, Spin-wave non-reciprocity in magnetization-graded ferromagnetic films, *New J. Phys.* **21**, 033026 (2019).
- [25] P. Borys, O. Kolokoltsev, N. Qureshi, M. L. Plumer, and T. L. Monchesky, Unidirectional spin wave propagation due to a saturation magnetization gradient, *Phys. Rev. B* **103**, 144411 (2021).
- [26] R. Macêdo, A. S. Kudinoor, K. L. Livesey, and R. E. Camley, Breaking Space Inversion-Symmetry to Obtain Asymmetric Spin-Wave Excitation in Systems with Nonuniform Magnetic Exchange, [arXiv:2012.10381](https://arxiv.org/abs/2012.10381).
- [27] A. V. Sadovnikov, E. N. Beginin, S. E. Sheshukova, Yu. P. Sharaevskii, A. I. Stognij, N. N. Novitski, V. K. Sakharov, Yu. V. Khivintsev, and S. A. Nikitov, Route toward semiconductor magnonics: Light-induced spin-wave nonreciprocity in a YIG/GaAs structure, *Phys. Rev. B* **99**, 054424 (2019).
- [28] S. Tateno and Y. Nozaki, Highly Nonreciprocal Spin Waves Excited by Magnetoelastic Coupling in a Ni/Si Bilayer, *Phys. Rev. Applied* **13**, 034074 (2020).
- [29] P. J. Shah, D. A. Bas, I. Lisenkov, A. Matyushov, N. X. Sun, and M. R. Page, Giant nonreciprocity of surface acoustic waves enabled by the magnetoelastic interaction, *Sci. Adv.* **6**, eabc5648 (2020).
- [30] X. Zhang, A. Galda, X. Han, D. Jin, and V. M. Vinokur, Broadband Nonreciprocity Enabled by Strong Coupling of Magnons and Microwave Photons, *Phys. Rev. Applied* **13**, 044039 (2020).
- [31] Y.-P. Wang, J. W. Rao, Y. Yang, P.-C. Xu, Y. S. Gui, B. M. Yao, J. Q. You, and C.-M. Hu, Nonreciprocity and Unidirectional Invisibility in Cavity Magnonics, *Phys. Rev. Lett.* **123**, 127202 (2019).
- [32] Q. Wang, M. Kewenig, M. Schneider, R. Verba, F. Kohl, B.

- Heinz, M. Geilen, M. Mohseni, B. Lagel, F. Ciubotaru, C. Adelman, C. Dubs, S. D. Cotozana, O. V. Dobrovolskiy, T. Bracher, P. Pirro and A. V. Chumak, A magnonic directional coupler for integrated magnonic half-adders, *Nat. Electron.* **3**, 765 (2020).
- [33] A. V. Chumak, A. A. Serga and B. Hillebrands, Magnon transistor for all-magnon data processing, *Nat. Commun.* **5**, 4700 (2014).
- [34] M. Mohseni, R. Verba, T. Bracher, Q. Wang, D. A. Bozhko, B. Hillebrands, and P. Pirro, Backscattering Immunity of Dipole-Exchange Magnetostatic Surface Spin Waves, *Phys. Rev. Lett.* **122**, 197201 (2019).
- [35] K. L. Wong, L. Bi, M. Bao, Q. Wen, J. P. Chatelon, Y.-T. Lin, C. A. Ross, H. Zhang, and K. L. Wang, Unidirectional propagation of magnetostatic surface spin waves at a magnetic film surface, *Appl. Phys. Lett.* **105**, 232403 (2014).
- [36] X. S. Wang, H. W. Zhang, and X. R. Wang, Topological Magnonics: A Paradigm for Spin-Wave Manipulation and Device Design, *Phys. Rev. Applied* **9**, 024029 (2018).
- [37] X. S. Wang, Y. Su, and X. R. Wang, Topologically protected unidirectional edge spin waves and beam splitter, *Phys. Rev. B* **95**, 014435 (2017).
- [38] Z.-X. Li, Y. Cao, and P. Yan, Topological insulators and semimetals in classical magnetic systems, *Phys. Rep.* **915**, 1 (2021).
- [39] Z.-X. Li, C. Wang, Y. Cao, and P. Yan, Edge states in a two-dimensional honeycomb lattice of massive magnetic skyrmions, *Phys. Rev. B* **98**, 180407(R) (2018).
- [40] A. Mook, J. Henk, and I. Mertig, Edge states in topological magnon insulators, *Phys. Rev. B* **90**, 024412 (2014).
- [41] R. Shindou, J. Ohe, R. Matsumoto, S. Murakami, and E. Saitoh, Chiral spin-wave edge modes in dipolar magnetic thin films, *Phys. Rev. B* **87**, 174402 (2013).
- [42] L. Udvardi and L. Szunyogh, Chiral Asymmetry of the Spin-Wave Spectra in Ultrathin Magnetic Films, *Phys. Rev. Lett.* **102**, 207204 (2009).
- [43] H. C. Wang, J. L. Chen, T. Liu, J. Y. Zhang, K. Baumgaertl, C. Y. Guo, Y. H. Li, C. P. Liu, P. Che, S. Tu, S. Liu, P. Gao, X. F. Han, D. P. Yu, M. Z. Wu, D. Grundler, and H. M. Yu, Chiral Spin-Wave Velocities Induced by All-Garnet Interfacial Dzyaloshinskii-Moriya Interaction in Ultrathin Yttrium Iron Garnet Films, *Phys. Rev. Lett.* **124**, 027203 (2020).
- [44] H. Bouloussa, Y. Roussigne, M. Belmeguenai, A. Stashkevich, S.-M. Cherif, S.D. Pollard, H. Yang, Dzyaloshinskii-Moriya interaction induced asymmetry in dispersion of magnonic Bloch modes, *Phys. Rev. B* **102**, 014412 (2020).
- [45] A. Hrabec, Z. Luo, L. J. Heyderman, and P. Gambardella, Chiral Spin-Wave Velocities Induced by All-Garnet Interfacial Dzyaloshinskii-Moriya Interaction in Ultrathin Yttrium Iron Garnet Films, *Appl. Phys. Lett.* **117**, 130503 (2020).
- [46] R. A. Gallardo, D. Cortes-Ortuno, T. Schneider, A. Roldan-Molina, F. Ma, R. E. Troncoso, K. Lenz, H. Fangohr, J. Lindner, and P. Landeros, Flat Bands, Indirect Gaps, and Unconventional Spin-Wave Behavior Induced by a Periodic Dzyaloshinskii-Moriya Interaction, *Phys. Rev. Lett.* **122**, 067204 (2019).
- [47] Y. Sun, H. Chang, M. Kabatek, Y.-Y. Song, Z. Wang, M. Jantz, W. Schneider, M. Wu, E. Montoya, B. Kardasz, B. Heinrich, S. G. E. te Velthuis, H. Schultheiss, and A. Hoffmann, Damping in Yttrium Iron Garnet Nanoscale Films Capped by Platinum, *Phys. Rev. Lett.* **111**, 106601 (2013).
- [48] Y. Au, E. Ahmad, O. Dmytriiev, M. Dvornik, T. Davison, and V. V. Kruglyak, Resonant microwave-to-spin-wave transducer, *Appl. Phys. Lett.* **100**, 182404 (2012).
- [49] Y. Au, M. Dvornik, O. Dmytriiev, and V. V. Kruglyak, Nanoscale spin wave valve and phase shifter, *Appl. Phys. Lett.* **100**, 172408 (2012).
- [50] J. L. Chen, T. Yu, C. P. Liu, T. Liu, M. Madami, K. Shen, J. Y. Zhang, S. Tu, M. S. Alam, K. Xia, M. Z. Wu, G. Gubbiotti, Y. M. Blanter, G. E. W. Bauer, and H. M. Yu, Excitation of unidirectional exchange spin waves by a nanoscale magnetic grating, *Phys. Rev. B* **100**, 104427 (2019).
- [51] H. Wang, J. Chen, T. Yu, C. Liu, C. Guo, S. Liu, K. Shen, H. Jia, T. Liu, J. Zhang, and M. A. Cabero, Nonreciprocal coherent coupling of nanomagnets by exchange spin waves, *Nano Res.* **14**, 2133 (2020).
- [52] J. Chen, J. Hu, and H. Yu, Chiral Emission of Exchange Spin Waves by Magnetic Skyrmions, *ACS Nano* **15**, 4372 (2021).
- [53] K. G. Fripp, A. V. Shytov, and V. V. Kruglyak, Spin-wave control using dark modes in chiral magnonic resonators, *Phys. Rev. B* **104**, 054437 (2021).
- [54] M. Sushruth, M. Grassi, K. Ait-Oukaci, D. Stoeffler, Y. Henry, D. Lacour, M. Hehn, U. Bhaskar, M. Bailleul, T. Devolder, and J.-P. Adam, Electrical spectroscopy of forward volume spin waves in perpendicularly magnetized materials, *Phys. Rev. Research* **2**, 043203 (2020).
- [55] V. F. Dmitriev and B. A. Kalinikos, Excitation of propagating magnetization waves by microstrip antennas, *Sov. Phys. J.* **31**, 875 (1988).
- [56] T. Schneider, A. A. Serga, T. Neumann, B. Hillebrands, and M. P. Kostylev, Phase reciprocity of spin-wave excitation by a microstrip antenna, *Phys. Rev. B* **77**, 214411 (2008).
- [57] V. E. Demidov, M. P. Kostylev, K. Rott, P. Krzysztoczko, G. Reiss, and S. O. Demokritov, Excitation of microwaveguide modes by a stripe antenna, *Appl. Phys. Lett.* **95**, 112509 (2009).
- [58] K. Kasahara, M. Nakayama, X. Ya, K. Matsuyama and T. Manago, Effect of distance between a magnet layer and an excitation antenna on the nonreciprocity of magnetostatic surface waves, *Jpn. J. Appl. Phys.* **56**, 010309 (2017).
- [59] H. M. Yu, O. D. Kelly, V. Cros, R. Bernard, P. Bortolotti, A. Anane, F. Brandl, F. Heimbach, and D. Grundler, Approaching soft X-ray wavelengths in nanomagnet-based microwave technology, *Nat. Commun.* **7**, 11255 (2016).
- [60] C. Liu, J. Chen, T. Liu, F. Heimbach, H. Yu, Y. Xiao, J. Hu, M. Liu, H. Chang, T. Stueckler, S. Tu, Y. Zhang, Y. Zhang, P. Gao, Z. Liao, D. Yu, K. Xia, N. Lei, W. Zhao, and M. Wu, Long-distance propagation of short-wavelength spin waves, *Nat. Commun.* **9**, 738 (2018).
- [61] P. Che, K. Baumgaertl, A. Kukolova, C. Dubs, and D. Grundler, Efficient wavelength conversion of exchange magnons below 100 nm by magnetic coplanar waveguides, *Nat. Commun.* **11**, 1445 (2020).
- [62] T. Yu, C. Liu, H. Yu, Y. M. Blanter, and G. E. W. Bauer, Chiral excitation of spin waves in ferromagnetic films by magnetic nanowire gratings, *Phys. Rev. B* **99**, 134424 (2019).
- [63] T. Yu, Y. M. Blanter, and G. E. W. Bauer, Chiral Pumping of Spin Waves, *Phys. Rev. Lett.* **123**, 247202 (2019).
- [64] D. D. Stancil and A. Prabhakar, *Spin Waves: Theory and Applications*. (Springer, New York, 2009).
- [65] A. Vansteenkiste, J. Leliaert, M. Dvornik, M. Helsen, F. Garcia-Sanchez, and B. Van Waeyenberge, The design and verification of MUMAX3, *AIP Adv.* **4**, 107133 (2014).
- [66] See Supplemental Material at [URL will be inserted by publisher] for the description of the simulation details (Sec. I), the derivation for the dipolar effects (Sec. II), dispersion relations with the mode profile (Sec. III), and the results for the right-hand and linear excitation (Sec. IV).
- [67] Z. Zhang, H. Yang, Z. Wang, Y. Cao, and P. Yan, Strong coupling of quantized spin waves in ferromagnetic bilayers, *Phys. Rev. B* **103**, 104420 (2021).

- [68] S. O. Demokritov, B. Hillebrands, and A. N. Slavin, Brillouin light scattering studies of confined spin waves: linear and nonlinear confinement, *Phys. Rep.* **348**, 441 (2001).
- [69] B. A. Kalinikos and A. N. Slavin, Theory of dipole-exchange spin wave spectrum for ferromagnetic films with mixed exchange boundary conditions, *J. Phys. C: Solid State Phys.* **19**, 7013 (2001).
- [70] T. Yu and G. E. W. Bauer, *Chiral coupling to magnetodipolar radiation*, *Top. Appl. Phys.* **138**, 1 (2021).
- [71] S. Yawale, S. Yawale, *Differential Amplifier. In: Operational Amplifier*. (Springer, Singapore, 2022).
- [72] S. V. Vasiliev, V. V. Kruglyak, M. L. Sokolovskii, and A. N. Kuchko, Spin wave interferometer employing a local nonuniformity of the effective magnetic field *J. Appl. Phys.* **101**, 113919 (2007).
- [73] M. P. Kostylev, A. A. Serga, T. Schneider, T. Neumann, B. Leven, B. Hillebrands, and R. L. Stamps, Resonant and nonresonant scattering of dipole-dominated spin waves from a region of inhomogeneous magnetic field in a ferromagnetic film *Phys. Rev. B* **76**, 184419 (2007).
- [74] S. O. Demokritov, A. A. Serga, A. André, V. E. Demidov, M. P. Kostylev, B. Hillebrands, and A. N. Slavin, Tunneling of Dipolar Spin Waves through a Region of Inhomogeneous Magnetic Field *Phys. Rev. Lett.* **93**, 047201 (2004).
- [75] M. Xu, K. Yamamoto, J. Puebla, K. Baumgaertl, B. Rana, K. Miura, H. Takahashi, D. Grundler, S. Maekawa, and Y. Otani, Nonreciprocal surface acoustic wave propagation via magneto-rotation coupling, *Sci. Adv.* **6**, eabb1724 (2020).
- [76] V. E. Demidov, S. Urazhdin, H. Ulrichs, V. Tiberkevich, A. Slavin, D. Baither, G. Schmitz and S. O. Demokritov, Magnetic nano-oscillator driven by pure spin current, *Nat. Mater.* **11**, 1028 (2012).
- [77] C. Safranski, I. Barsukov, H. K. Lee, T. Schneider, A. A. Jara, A. Smith, H. Chang, K. Lenz, J. Lindner, Y. Tserkovnyak, M. Wu and I. N. Krivorotov, Spin caloritronic nano-oscillator, *Nat. Commun.* **8**, 117 (2017).
- [78] Z. Zhang, M. Vogel, J. Holanda, M. B. Jungfleisch, C. Liu, Y. Li, J. E. Pearson, R. Divan, W. Zhang, A. Hoffmann, Y. Nie, and V. Novosad, Spin-wave frequency division multiplexing in an yttrium iron garnet microstripe magnetized by inhomogeneous field, *Appl. Phys. Lett.* **115**, 232402 (2019).

# Supplemental Material

## Nonreciprocal Spin Waves Driven by Left-Hand Microwaves

Zhizhi Zhang, Zhenyu Wang, Huanhuan Yang, Z.-X. Li, Yunshan Cao, and Peng Yan

*School of Electronic Science and Engineering and State Key Laboratory of Electronic Thin Films and Integrated Devices, University of Electronic Science and Technology of China, Chengdu 610054, China*

### I. MICROMAGNETIC SIMULATIONS

MuMax 3.0 open source GPU-based software is utilized, which numerically solves the Landau-Lifshitz-Gilbert equation. The magnetic parameters of YIG are used, which are:  $M_s = 1.48 \times 10^5$  A/m,  $A_{ex} = 3.1 \times 10^{-12}$  J/m, and  $\alpha = 5 \times 10^{-4}$ . The systems are meshed by cells with dimensions equal to  $2 \times 2 \times 100$  nm<sup>3</sup>. Periodic boundary conditions (PBC  $\times 200$ ) in the  $z$  direction are applied, which means that the film is practically infinite in the  $z$  direction. The absorption boundary conditions are applied by adding the attenuating areas where the  $\alpha$  is gradually increasing to 0.25 to avoid the reflection at the two ends of simulated systems. In the dispersion relation calculation, the length of the simulated YIG film is  $50 \mu\text{m}$ , with the narrow enough excitation width  $w = 10$  nm for a broad wave vector range. The excitation is applied in the excitation area ( $w = 10$  nm) using a ‘‘sinc’’ function  $\mathbf{h}_{rf}(t) = h_0 \sin[\omega_f(t - t_0)]/[\omega_f(t - t_0)]\hat{\mathbf{x}}$  with the cut-off frequency  $\omega_f/2\pi = 50$  GHz,  $t_0 = 0.5$  ns, and  $h_0 = 1$  mT. The total simulation time is 200 ns, and the results record the dynamic normalized magnetization ( $m_y/M_s$ ) evolution as a function of time and position along  $x$  direction. The dispersion relations were obtained through the two-dimensional FFT (2D-FFT) operation on  $m_y/M_s$  [1]. In the chiral excitation simulations with fixed frequency, the excitation is applied using the function  $\mathbf{h}_{rf}(t) = h_{x0} \sin(\omega t)\hat{\mathbf{x}} + h_{y0} \sin(\omega t \pm \pi/2)\hat{\mathbf{y}}$ , with ‘‘+’’ (‘‘-’’) for the left (right) hand polarization, where  $h_{x0}$  and  $h_{y0}$  satisfy  $h_{x0}^2 + h_{y0}^2 = (0.1 \text{ mT})^2$  and  $h_{x0}/h_{y0} = |\varepsilon_h|$  to ensure the same RF power density with different  $|\varepsilon_h|$ . The results record the dynamic normalized magnetization ( $m_x/M_s$  and  $m_y/M_s$ ) evolution as a function of time and space.

### II. DIPOLAR EFFECT

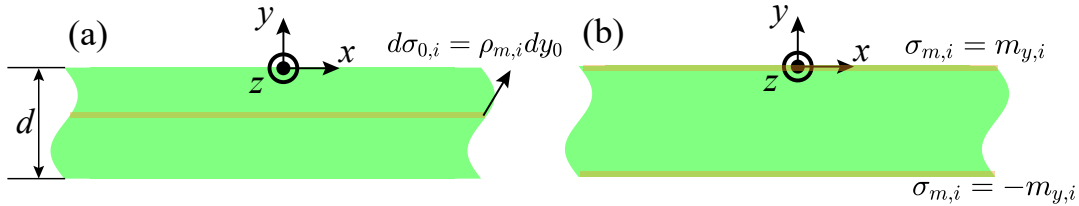


FIG. S1: Schematics of the effective (a) *volume* and (b) *surface* magnetic-charges. The patched yellow parts represent the differential elements

In this section, we investigate the dipolar effects induced by the spin waves (SWs) propagating in the ultra thin magnetic film. The dipolar field in the whole space is calculated. The self and mutual demagnetizing factors are figured out in Sec. II A and Sec. II B, respectively.

We considered a magnetic film extended infinitely along  $x$  and  $z$  directions, located from  $y = -d$  to  $0$  and labelled as  $L_i$ . The SWs takes the form  $\mathbf{m}_i = \mathbf{m}_{0,i} e^{j(\omega t - k_x x)} = m_{x,i} \hat{\mathbf{x}} + m_{y,i} \hat{\mathbf{y}}$  with  $\mathbf{m}_{0,i} = m_{x0,i} \hat{\mathbf{x}} + m_{y0,i} \hat{\mathbf{y}}$ . The dynamic magnetization  $\mathbf{m}_i$  and the correspondingly induced dipolar field  $\mathbf{h}_{d,i}$  satisfy the magnetostatic equations:

$$\nabla \cdot (\mathbf{h}_{d,i} + \mathbf{m}_i) = 0, \quad (1a)$$

$$\nabla \times \mathbf{h}_{d,i} = 0. \quad (1b)$$

Introducing the scale potential  $\psi_{m,i}$ , we have:

$$\mathbf{h}_{d,i} = -\nabla \psi_{m,i}. \quad (2)$$

Then Eq. (1a) becomes Poisson equation:

$$\nabla^2 \psi_{m,i} = -\rho_i, \quad (3)$$



where  $\rho_i$  is the effective magnetic-charge density, given as:

$$\rho_i = -\nabla \cdot \mathbf{m}_i. \quad (4)$$

One crucial step is to find the solution of  $\psi_{m,i}$  in Eq. (3). We note that there are two contributions to  $\psi_{m,i}$  in magnetic materials: effective *volume* magnetic-charge density  $\rho_{m,i}$  and effective *surface* magnetic-charge density  $\sigma_{m,i}$  [2].

Firstly, we calculate the contribution of  $\rho_{m,i}$ . Inside the film,  $\rho_{m,i} = -\nabla \cdot \mathbf{m}_i = jk_x m_{x,i}$  is induced by the  $x$  component of  $m_i$  [3]. To begin with, we consider a tiny sheet of film located at position  $y = y_0$  with thickness  $dy_0$ , whose surface magnetic charge density is  $\sigma_{0,i} = \rho_{m,i} dy_0$  [see Fig. S1(a)]. The magnetostatic potential  $\psi_{m,i}(\sigma_{0,i}, y_0, \mathbf{r}, t)$  induced by  $\sigma_{0,i}$  is periodic (evanescent) along  $x$  ( $y$ ) direction, while its maximum locates at  $y = y_0$  and satisfy Laplace equation  $\nabla^2 \psi_{m,i}(\sigma_{0,i}, y_0, \mathbf{r}, t) = 0$  [4]. Then the solution can be expressed as:

$$\psi_{m,i}(\sigma_{0,i}, y_0, \mathbf{r}, t) = \psi_{m0,i}(\sigma_{0,i}) e^{-|k_x(y-y_0)|} e^{j(\omega t - k_x x)}. \quad (5)$$

The next important step is to find out the value of  $\psi_{m0,i}$ . Note that the boundary condition (continuity of  $B_y$ ) of the tiny sheet is given as:

$$h_{y,i}(\sigma_{0,i}, y_0^+, \mathbf{r}, t) - h_{y,i}(\sigma_{0,i}, y_0^-, \mathbf{r}, t) = \sigma_{0,i}. \quad (6)$$

Using Eq. (2), we have:

$$h_{y,i}(\sigma_{0,i}, y_0, \mathbf{r}, t) = -\frac{\partial}{\partial y} \psi_{m,i}(\sigma_{0,i}, y_0, \mathbf{r}, t) = \begin{cases} |k_x| \psi_{m0,i} e^{k_x(y-y_0)} e^{j(\omega t - k_x x)}, & y \geq y_0 \\ |k_x| \psi_{m0,i} e^{-k_x(y-y_0)} e^{j(\omega t - k_x x)}, & y < y_0 \end{cases}. \quad (7)$$

Therefore, we have:

$$2|k_x| \psi_{m0,i}(\sigma_{0,i}) e^{j(\omega t - k_x x)} = \sigma_{0,i}. \quad (8)$$

The magneto-static potential induced by the sheet at  $y = y_0$  can be expressed as:

$$\psi_{m,i}(\sigma_{0,i}, y_0, \mathbf{r}, t) = \frac{j \text{sgn}(k_x) m_{x0,i} e^{j(\omega t - k_x x)}}{2} e^{-|k_x y - y_0|} dy_0. \quad (9)$$

Correspondingly, the dipolar magnetic field  $\mathbf{h}_{d,i}(\sigma_{0,i}, y_0, \mathbf{r}, t)$  derived from  $\psi_{m,i}(\sigma_{0,i}, y_0, \mathbf{r}, t)$  is given as:

$$\mathbf{h}_{d,i}(\sigma_{0,i}, y_0, \mathbf{r}, t) = \frac{j \text{sgn}(k_x) m_{x,i}}{2} e^{-|k_x y - y_0|} [-\text{sgn}(k_x) \hat{\mathbf{x}} + j \text{sgn}(y - y_0) \hat{\mathbf{y}}] dy_0. \quad (10)$$

The dipolar field  $\mathbf{h}_{d,i}(\rho_{m,i}, \mathbf{r}, t)$  induced by  $\rho_{m,i}$  at any position  $\mathbf{r}$  is given:

$$\begin{aligned} \mathbf{h}_{d,i}(\rho_{m,i}, \mathbf{r}, t) &= \frac{1}{2} \int_{-d}^0 j \text{sgn}(k_x) m_{x,i} e^{-|k_x y - y_0|} [-\text{sgn}(k_x) \hat{\mathbf{x}} + j \text{sgn}(y - y_0) \hat{\mathbf{y}}] dy_0 \\ &= \begin{cases} \frac{m_{x,i}}{2} e^{-|k_x|y} (1 - e^{-|k_x|d}) [-\hat{\mathbf{x}} + j \text{sgn}(k_x) \hat{\mathbf{y}}], & y \geq 0 \\ -\frac{m_{x,i}}{2} [2 - e^{-|k_x|(y+d)} - e^{|k_x|y}] \hat{\mathbf{x}} + \frac{j m_{x,i}}{2} \text{sgn}(k_x) [e^{|k_x|y} - e^{-|k_x|(y+d)}] \hat{\mathbf{y}}, & -d \leq y < 0 \\ \frac{m_{x,i}}{2} e^{|k_x|y} (e^{|k_x|d} - 1) [-\hat{\mathbf{x}} - j \text{sgn}(k_x) \hat{\mathbf{y}}], & y < -d \end{cases} \end{aligned} \quad (11)$$

Next, we calculate the contribution of  $\sigma_{m,i} = \mathbf{m}_i \cdot \hat{\mathbf{n}}$ , located only at the position  $y = 0$  and  $y = -d$  with  $\hat{\mathbf{n}}$  the unit vector normal to the surface. They are equal to  $m_{y,i} = m_{y0,i} e^{j(\omega t - k_x x)}$  and  $-m_{y,i}$ , where the minus sign comes from the opposite directions of the top and bottom surfaces. Following the steps from Eqs. (5) to (9), we obtain the magneto-static potential induced by  $\sigma_{m,i}$ :

$$\psi_{m,i}(\sigma_{m,i}, 0, \mathbf{r}, t) = \frac{m_{y0,i}}{2|k_x|} e^{j(\omega t - k_x x)} e^{-|k_x y|}, \quad (12a)$$

$$\psi_{m,i}(\sigma_{m,i}, -d, \mathbf{r}, t) = -\frac{m_{y0,i}}{2|k_x|} e^{j(\omega t - k_x x)} e^{-|k_x(y+d)|}. \quad (12b)$$

The dipolar field  $\mathbf{h}_{d,i}(\sigma_{m,i}, \mathbf{r}, t)$  induced by  $\sigma_{m,i}$  at any position  $\mathbf{r}$  is given [3]:

$$\mathbf{h}_{d,i}(\sigma_{m,i}, \mathbf{r}, t) = -\nabla [\psi_{m,i}(\sigma_{m,i}, 0, \mathbf{r}, t) + \psi_{m,i}(\sigma_{m,i}, -d, \mathbf{r}, t)]$$

$$= \begin{cases} \frac{m_{y,i}}{2} e^{-|k_x|y} (1 - e^{-|k_x|d}) [j\text{sgn}(k_x)\hat{\mathbf{x}} + \hat{\mathbf{y}}], & y \geq 0 \\ -\frac{j m_{y,i}}{2} [e^{|k_x|y} - e^{-|k_x|(y+d)}] \text{sgn}(k_x)\hat{\mathbf{x}} + \frac{m_{y,i}}{2} [-e^{-|k_x|(y+d)} - e^{|k_x|y}] \hat{\mathbf{y}}, & -d \leq y < 0 \\ \frac{m_{y,i}}{2} e^{|k_x|y} (e^{|k_x|d} - 1) [-j\text{sgn}(k_x)\hat{\mathbf{x}} + \hat{\mathbf{y}}]. & y < -d \end{cases} \quad (13)$$

Finally, we obtain the dipolar magnetic field  $\mathbf{h}_{d,i}(\mathbf{r}, t) = \mathbf{h}_{d,i}(\rho_{m,i}, \mathbf{r}, t) + \mathbf{h}_{d,i}(\sigma_{m,i}, \mathbf{r}, t)$  in the whole space:

$$\mathbf{h}_{d,i}(\mathbf{r}, t) = \begin{cases} \frac{1}{2} e^{-|k_x|y} (1 - e^{-|k_x|d}) \left\{ [-m_{x,i} + j\text{sgn}(k_x)m_{y,i}] \hat{\mathbf{x}} + [j\text{sgn}(k_x)m_{x,i} + m_{y,i}] \hat{\mathbf{y}} \right\}, & y \geq 0 \\ \left\{ [e^{-|k_x|(y+d)} + e^{|k_x|y} - 2] \frac{m_{x,i}}{2} + \frac{j\text{sgn}(k_x)}{2} [e^{-|k_x|(y+d)} - e^{-|k_x|y}] m_{y,i} \right\} \hat{\mathbf{x}} \\ + \left\{ \frac{j\text{sgn}(k_x)}{2} [e^{|k_x|y} - e^{-|k_x|(y+d)}] m_{x,i} - [e^{-|k_x|y} + e^{-|k_x|(y+d)}] \frac{m_{y,i}}{2} \right\} \hat{\mathbf{y}}, & -d \leq y < 0 \\ \frac{1}{2} e^{|k_x|y} (e^{|k_x|d} - 1) \left\{ [-m_{x,i} - j\text{sgn}(k_x)m_{y,i}] \hat{\mathbf{x}} + [-j\text{sgn}(k_x)m_{x,i} + m_{y,i}] \hat{\mathbf{y}} \right\}, & y < -d \end{cases} \quad (14)$$

#### A. Self demagnetizing factors

When calculating the demagnetizing factor of a single layer with thickness  $d_i$ , we care about the region  $-d_i < y < 0$ . The demagnetizing factors inside the film are defined as the ratios between the average dipolar field and the magnetization:

$$-n_{x,i} m_{x,i} = \frac{1}{d} \int_{-d}^0 \hat{\mathbf{x}} \cdot \mathbf{h}_{d,i}(\mathbf{r}, t) dy, \quad (15a)$$

$$-n_{y,x} m_{x,i} = \frac{1}{d} \int_{-d}^0 \hat{\mathbf{y}} \cdot \mathbf{h}_{d,i}(\mathbf{r}, t) dy, \quad (15b)$$

$$-n_{x,y} m_{x,i} = \frac{1}{d} \int_{-d}^0 \hat{\mathbf{x}} \cdot \mathbf{h}_{d,i}(\mathbf{r}, t) dy, \quad (15c)$$

$$-n_{y,i} m_{x,i} = \frac{1}{d} \int_{-d}^0 \hat{\mathbf{y}} \cdot \mathbf{h}_{d,i}(\mathbf{r}, t) dy. \quad (15d)$$

We obtain:

$$n_{x,i} = 1 - n_{y,i} = 1 - \frac{1 - e^{-|k_x|d_i}}{|k_x|d_i} \quad (16a)$$

$$n_{xy} = n_{yx} = 0. \quad (16b)$$

The net self-induced dipolar field  $\mathbf{h}_{d, self, i} = h_{d, self, x} \hat{\mathbf{x}} + h_{d, self, y} \hat{\mathbf{y}}$  by the SWs can be evaluated:

$$\begin{bmatrix} h_{d, self, x} \\ h_{d, self, y} \end{bmatrix} = - \begin{bmatrix} n_{x,i} & 0 \\ 0 & n_{y,i} \end{bmatrix} \begin{bmatrix} m_{x,i} \\ m_{y,i} \end{bmatrix}. \quad (17)$$

The ratio  $\varepsilon_{hd}$  between  $h_{d,x}$  and  $h_{d,y}$  is given as:

$$\varepsilon_{hd} = \frac{h_{d,x}}{h_{d,y}} = \frac{n_{x,i} m_{x,i}}{n_{y,i} m_{y,i}}, \quad (18)$$

indicating that the chirality of the self-induced dipolar field depends on the chirality of the dynamic magnetization.

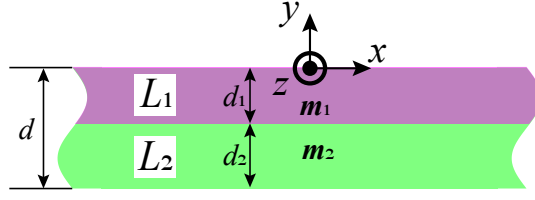


FIG. S2: Schematic of the bilayer consisted of  $L_1$  (purple) and  $L_2$  (green) with SWs  $\mathbf{m}_1$  and  $\mathbf{m}_2$  inside, respectively

### B. Mutual demagnetizing effects

In this part, we consider the dipolar effects between the two adjacent layers labelled as  $L_1$  and  $L_2$ , as shown in Fig. S2. They are located from  $y = -d_1$  to  $0$  and from  $y = -d$  to  $-d_1$ , respectively. For simplification, we denote  $d_2 = d - d_1$ . The SWs propagating inside take the form  $\mathbf{m}_p = \mathbf{m}_{0,p} e^{j(\omega t - k_x p x)} = m_{x,p} \hat{\mathbf{x}} + m_{y,p} \hat{\mathbf{y}}$  with  $p = 1, 2$ . According to Eq. (14), the dipolar field induced by  $\mathbf{m}_1$  and acting on  $L_2[-(d_1 + d_2) < y < -d_1]$  is given as:

$$\mathbf{h}_{d,12}(\mathbf{r}, t) = \frac{1}{2} e^{k_{x,1}|y|} \left( e^{k_{x,1}|d_1|} - 1 \right) \left\{ \left[ -m_{x,1} - j \operatorname{sgn}(k_{x,1}) m_{y,1} \right] \hat{\mathbf{x}} + \left[ -j \operatorname{sgn}(k_{x,1}) m_{x,1} + m_{y,1} \right] \hat{\mathbf{y}} \right\}. \quad (19)$$

The average dipolar field acting on  $L_2$  can be evaluated by introducing the mutual demagnetizing factors  $n_{x12}$ ,  $n_{xy12}$ ,  $n_{yx12}$  and  $n_{y12}$ :

$$-n_{x12} m_{x,1} - n_{xy12} m_{y,1} = \frac{1}{d_2} \int_{-(d_1+d_2)}^{-d_1} \hat{\mathbf{x}} \cdot \mathbf{h}_{d,12}(\mathbf{r}, t) dy, \quad (20a)$$

$$-n_{yx12} m_{x,1} - n_{y12} m_{y,1} = \frac{1}{d_2} \int_{-(d_1+d_2)}^{-d_1} \hat{\mathbf{y}} \cdot \mathbf{h}_{d,12}(\mathbf{r}, t) dy. \quad (20b)$$

We obtain:

$$n_{x12} = -n_{y12} = \frac{(1 - e^{-k_{x,1}|d_1|})(1 - e^{-k_{x,1}|d_2|})}{2|k_{x,1}|d_2}, \quad (21a)$$

$$n_{xy12} = n_{yx12} = j \operatorname{sgn}(k_{x,1}) n_{x12}. \quad (21b)$$

The dipolar field induced by  $\mathbf{m}_2$  and acting on  $L_1(-d_1 < y < 0)$  is given as:

$$\mathbf{h}_{d,21}(\mathbf{r}, t) = \frac{1}{2} e^{-k_{x,2}(y+d_1)} \left( 1 - e^{-k_{x,2}|d_2|} \right) \left\{ \left[ -m_{x,2} + j \operatorname{sgn}(k_{x,2}) m_{y,2} \right] \hat{\mathbf{x}} + \left[ j \operatorname{sgn}(k_{x,2}) m_{x,1} + m_{y,2} \right] \hat{\mathbf{y}} \right\}. \quad (22)$$

We note that  $y \rightarrow y + d_1$  in Eq. (22) compared with Eq. (14) because  $L_2$  is shifted downward by  $d_1$ . Similarly, we introduce  $n_{x21}$ ,  $n_{xy21}$ ,  $n_{yx21}$  and  $n_{y21}$ :

$$-n_{x21} m_{x,1} - n_{xy21} m_{y,1} = \frac{1}{d_1} \int_{-d_1}^0 \hat{\mathbf{x}} \cdot \mathbf{h}_{d,21}(\mathbf{r}, t) dy, \quad (23a)$$

$$-n_{yx21} m_{x,1} - n_{y21} m_{y,1} = \frac{1}{d_1} \int_{-d_1}^0 \hat{\mathbf{y}} \cdot \mathbf{h}_{d,21}(\mathbf{r}, t) dy. \quad (23b)$$

We obtain:

$$n_{x21} = -n_{y21} = \frac{(1 - e^{-k_{x,2}|d_1|})(1 - e^{-k_{x,2}|d_2|})}{2|k_{x,2}|d_1}, \quad (24a)$$

$$n_{xy21} = n_{yx21} = -j \operatorname{sgn}(k_{x,2}) n_{x21}. \quad (24b)$$

Finally, the mutual net dipolar field  $\mathbf{h}_{d,12} = h_{d,x,12} \hat{\mathbf{x}} + h_{d,y,12} \hat{\mathbf{y}}$  and  $\mathbf{h}_{d,21} = h_{d,x,21} \hat{\mathbf{x}} + h_{d,y,21} \hat{\mathbf{y}}$  can be evaluated:

$$\begin{bmatrix} h_{d,x,12} \\ h_{d,y,12} \end{bmatrix} = -n_{x12} \begin{bmatrix} 1 & j \operatorname{sgn}(k_{x,1}) \\ j \operatorname{sgn}(k_{x,1}) & -1 \end{bmatrix} \begin{bmatrix} m_{x,1} \\ m_{y,1} \end{bmatrix}. \quad (25)$$

And:

$$\begin{bmatrix} h_{d,x,21} \\ h_{d,y,21} \end{bmatrix} = -n_{x21} \begin{bmatrix} 1 & -j\text{sgn}(k_{x,2}) \\ -j\text{sgn}(k_{x,2}) & -1 \end{bmatrix} \begin{bmatrix} m_{x,2} \\ m_{y,2} \end{bmatrix}. \quad (26)$$

The ratio  $\varepsilon_{hd12}$  ( $\varepsilon_{hd21}$ ) between  $h_{d,x,12}$  and  $h_{d,y,12}$  ( $h_{d,x,21}$  and  $h_{d,y,21}$ ) is given as:

$$\varepsilon_{hd12} = \frac{m_{x,1} + j\text{sgn}(k_{x,1})m_{y,1}}{j\text{sgn}(k_{x,1})m_{x,1} - m_{y,1}} = -j\text{sgn}(k_{x,1}), \quad (27a)$$

$$\varepsilon_{hd21} = \frac{m_{x,2} - j\text{sgn}(k_{x,2})m_{y,2}}{-j\text{sgn}(k_{x,2})m_{x,2} + m_{y,2}} = j\text{sgn}(k_{x,2}). \quad (27b)$$

indicating that the chirality of the mutual dipolar field depends on the signs of the wave vectors. The net mutual demagnetizing field can be estimated as:

$$\begin{aligned} \mathbf{h}_{d,mut} &= \frac{\mathbf{h}_{d,12}d_2 + \mathbf{h}_{d,21}d_1}{d} \\ &= -\frac{(1 - e^{-|k_{x,2}|d_1})(1 - e^{-|k_{x,2}|d_2})}{2|k_x|d} \left\{ [(m_{x,1} + m_{x,2}) + j\text{sgn}(k_x)(m_{y,1} - m_{y,2})] \hat{\mathbf{x}} + [j\text{sgn}(k_x)(m_{x,1} - m_{x,2}) - (m_{y,1} + m_{y,2})] \hat{\mathbf{y}} \right\}. \end{aligned} \quad (28)$$

Here, we note that in the main text, the dynamic magnetization  $\mathbf{m}_1$  and  $\mathbf{m}_2$  satisfy the boundary condition  $\mathbf{m}_1 = \mathbf{m}_2 \Big|_{y=-d_1}$  [5], which gives  $k_{x,1} = k_{x,2} = k_x$

### III. DISPERSION RELATION

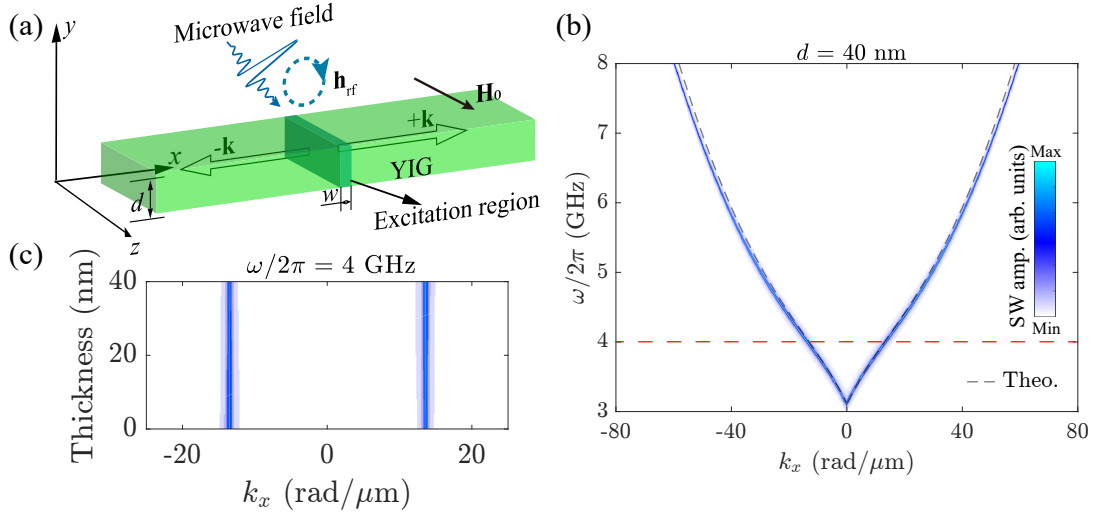


FIG. S3: (a) Schematic of the chiral excitation of SWs with a coordinate system and geometric parameters. The chiral microwave field  $\mathbf{h}_{rf}$  is locally applied in the patched green region. The SWs are propagating along  $x$  direction indicated by the hollow arrows. (b) Color plot of the SW dispersion relation of the film ( $d = 40$  nm) obtained from micromagnetic simulation. The dashed black line show the dispersion curve of the first unpinned exchange mode predicted by Eq. (4) in main text with  $H_0$  fixed at 52 mT (same hereinafter). (c) SW profiles across the thickness at 4 GHz, indicated by the horizontal dashed red line in (b).

The magnetization dynamics is governed by Landau-Lifshitz-Gilbert (LLG) equation:

$$\frac{\partial \mathbf{M}}{\partial t} = -\gamma \mu_0 \mathbf{M} \times \mathbf{H}_{\text{eff}} + \frac{\alpha}{M_s} \mathbf{M} \times \frac{\partial \mathbf{M}}{\partial t}, \quad (29)$$

To calculate the dispersion relation, we neglect the damping term and set  $\mathbf{h}_{rf} = 0$ , indicating that the SWs can propagate far away from excitation, and assume a plane-wave form  $\mathbf{m} = \mathbf{m}_0 e^{j(\omega t - k_x x)}$  with  $\mathbf{m}_0 = m_{x0} \mathbf{x} + m_{y0} \mathbf{y}$  and  $m_{x(y)} = m_{x0(y0)} e^{j(\omega t - k_x x)}$ .



Substituting these terms into Eq. (29) and adopting the linear approximation, we obtain

$$j\omega m_x + \omega_y m_y = 0, \quad (30a)$$

$$-\omega_x m_x + j\omega m_y = 0, \quad (30b)$$

where  $\omega_x = n_x \omega_M + \omega_H + \omega_{ex}$  and  $\omega_y = n_y \omega_M + \omega_H + \omega_{ex}$ , with  $\omega_M = \gamma \mu_0 M_s$ ,  $\omega_H = \gamma \mu_0 H_0$ , and  $\omega_{ex} = (2\gamma A/M_s)k_x^2$ . The SW dispersion relation with  $d = 40$  nm and  $H_0 = 52$  mT (same with those in the main text) obtained from simulation shows only one band exists in the low frequency range from 3 to 8 GHz [see Fig. S3(b)], whose profile across the thickness is uniform [see Fig. S3(c)].

#### IV. SPECTRA FOR THE RIGHT-HAND AND LINEAR EXCITATIONS

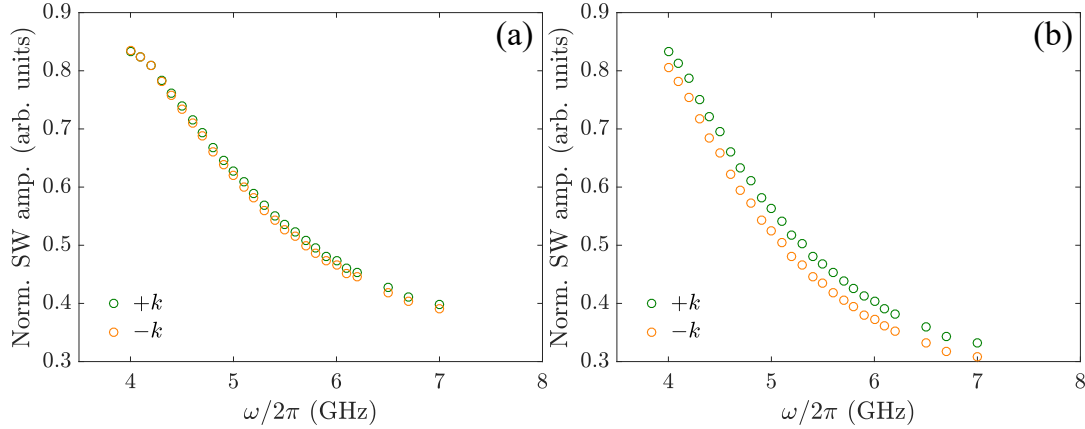


FIG. S4: Forward (green symbols) and backward (orange symbols) SW spectra under the right-hand (a) and linear (b) excitations unevenly applied across the film thickness.

Figures S4 show the simulated spectra of the SWs excited by the right-hand and linear microwaves applied unevenly across the film thickness with  $d_1 = 10$  nm, as shown in Fig. 4 in the main text. The results indicate that the Damon-Eschbach mechanism contributes negligibly to the non-reciprocity in this work.

- 
- [1] D. Kumar, O. Dmytriiev, S. Ponraj, and A. Barman, Numerical calculation of spin wave dispersions in magnetic nanostructures, *J. Phys. D* **45**, 015001 (2011).
  - [2] J. D. Jackson, *Classical Electrodynamics*, (Wiley, New York, 1962).
  - [3] Y. Henry, O. Gladii, and M. Bailleul, Propagating spin-wave normal modes: A dynamic matrix approach using plane-wave demagnetizing tensors, [arXiv:1611.06153](https://arxiv.org/abs/1611.06153).
  - [4] M. Bailleul, Spectroscopie d'ondes de spin pour l'électronique de spin, Habilitation thesis, University of Strasbourg (2011).
  - [5] R. Verba, V. Tiberkevich, and A. Slavin, Spin-wave transmission through an internal boundary: Beyond the scalar approximation, *Phys. Rev. B* **101**, 144430 (2020).